ACS OMEGA

http://pubs.acs.org/journal/acsodf

Article

Preparation and Characterization of Electric Double-Layer Capacitors Having a 3D Stainless-Steel Fiber Sheet as the Current Collector

Daisuke Muramatsu, Keisuke Masunaga, Aoi Magori, Satoru Tsukada, and Katsuyoshi Hoshino*

Cite This: *ACS Omega* 2022, 7, 19216−19224

Read Online

ACCESS | Metrics & More | Article Recommendations | Supporting Information

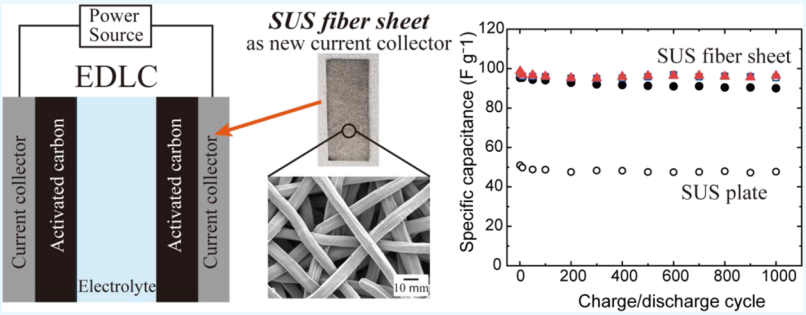

ABSTRACT: One strategy to improve the performance of electric double-layer capacitors (EDLCs) is changing the current collector material. In this study, a three-dimensional porous current collector comprising stainless-steel fibers is fabricated using a relatively simple method. Capacitor properties of the EDLC using this unique current collector are characterized by cyclic voltammetry and charge−discharge tests. The voltammograms of the EDLC develop a more butterfly shape and an increased specific capacity at higher electrolyte concentrations. It shows reversible charge−discharge potential profiles, little capacity degradation (~98% of the initial capacity at 1000th cycle), and a good rate performance at higher electrolyte concentrations (90% capacity retention for 2.5 times increase in discharge current). Its capacitance values (95−99 F g^{-1}) are roughly twice the specific capacitance of an EDLC using the flat stainless-steel plate current collector (51 F g^{-1}) without any performance degradation even at a higher loading of electrode active materials. Based on the AC impedance analysis, these good properties are attributed to the reduction in several resistances compared to the case of a flat stainless-steel plate: (i) the contact resistance between the electrode active material and the current collector, (ii) the resistance of the electrolyte in the finely branched space formed by the fibers and the active material, and (iii) the resistance in the diffusion layer. Increasing the electrolyte concentration further reduces the latter two resistances and the bulk electrolyte resistance, resulting in higher performance of the EDLC using the stainless-steel fiber sheet current collector.

1. INTRODUCTION

With the growing popularity of electronic devices such as smart phones and the development of electric vehicles, there is sustained research interest in energy storage devices. Electrochemical capacitors, which are typical of electric double-layer capacitors (EDLCs),[1,2] have been applied in various industrial products, including emergency power supplies, auxiliary power supplies, and high-power compact power supplies.[3,4] During charging and discharging, EDLCs do not experience chemical reactions but rather undergo electrostatic charge separation in the electric double layer formed between the electrode and the electrolyte. Therefore, they are theoretically capable of rapid, high-current charging/discharging and have a long life. This potential has motivated researchers to keep improving the performance of EDLCs.

The structure of an EDLC can be roughly divided into three parts: the electrode, the electrolyte, and the separator. The electrode is composed of (i) active materials that form the electric double layer, (ii) conductive assistants to create a conductive network, and (iii) binders to hold everything together. The electrode layer is supported by the current collector, which is the path for current flow between the electrode layer and the tab lead. For the electrode layer, studies have been conducted on the pore size of activated carbon as active materials[5,6] and using graphene[7−9] and carbon nanotubes[9−13] as conductive assistants. Some reported supercapacitors used conductive assistants as the active materials

Received: January 21, 2022
Accepted: May 13, 2022
Published: May 27, 2022

and achieved better performance than conventional EDLCs.[14−16] The electrolyte has also been actively investigated because of its major role in controlling the operating voltage and solution resistance of EDLCs. For example, organic[17] or gel electrolytes[18−23] could be used to extend the working voltage range.

Compared to the active materials and electrolyte, fewer studies have focused on the current collector.[24] While aluminum or stainless-steel (SUS) foils are commonly used as current collectors,[25] certain metal foams fabricated using a specialized metal plating process were reported to improve the charge−discharge characteristics. For example, nickel foams have been used as current collectors in nickel−metal hydride batteries for portable devices and potassium-ion batteries.[26−29] The three-dimensional (3D) structure of the nickel foam improves the interaction between the diffused electrolyte ion and the substrate because the foam has a larger effective surface area than a flat substrate. The nickel foam also provides a network for efficient electron collection and excellent channels for ion diffusion. In addition, this material is chemically stable in many liquid electrolytes and therefore is considered an excellent current collector.[27,28] Nickel−chromium alloy foam current collectors were also reported to improve the high-rate discharging capability of EDLCs.[30] Furthermore, porous aluminum[31] or aluminum foam[32,33] current collectors have been developed in recent years because aluminum has high electrical conductivity, low mass density, good stability under high voltage, and abundant resource reserves. When used in capacitors and batteries, these aluminum-based materials were found to exhibit good rate characteristics and charge−discharge cycle characteristics. In addition, interesting examples include the use of picosecond laser-treated Al foil with hierarchical micro−nanostructures and porous carbon sheets prepared by electrospinning for the current collectors of EDLCs, which showed good capacitor performances.[24,34]

In this study, we used a novel, facile method to fabricate a porous metal current collector without metal plating. In particular, SUS, which is used as one of the current collector materials as described above, was selected and its fiber sheet was prepared by bonding the contacts within a nonwoven fabric of SUS fibers. EDLCs using this SUS fiber sheet as the current collector showed superior capacitor performances compared to those using a flat SUS plate.

2. EXPERIMENTAL SECTION

2.1. Fabrication of the SUS Fiber Sheet. SUS fibers (SUS316L) were produced by Bekaert Co. using the converging wire drawing method. These fibers have an average diameter of 8.0 μm, an average length of 3.0 mm, and irregularly shaped cross sections. The SUS fibers and polyvinyl alcohol fibers[35,36] (Fibribond VPB105, Kuraray Co., Ltd.) were codispersed at a weight ratio of 98:2 in water to produce the slurry. After removing the layer containing a higher concentration of SUS fibers at the bottom of the agitator, the rest of the slurry was filtered through a papermaking screen, and the solid layer was dehydrated on the screen to form sheets. These sheets were dried at 140 °C in a dryer to obtain a nonwoven fabric comprising of SUS and polyvinyl alcohol fibers. After the fabric has been compressed at room temperature and at a linear pressure of 80 kg cm^{-1}, it was later sintered at 1120 °C for 60 min in an atmosphere of 75% H_2 and 25% N_2 gases in order to remove polyvinyl alcohol and as well bond the contacts between the SUS fibers. The sintered SUS sheet was cooled to room temperature and pressed at a linear pressure of 240 kg cm^{-1} to obtain the SUS fiber sheet. The SUS fiber sheet had a basis weight of 300 g m^{-2}, a thickness of 111 μm, and an average occupancy of 33.7% (or a porosity of 66.3%). Morphological observations and sheet resistance measurement of the SUS fiber sheet were carried out using a scanning electron microscope (SEM, JSM-6510A, JEOL) and a resistivity meter (Loresta-GP MCP-T600 with an MCP-TP06P probe, Mitsubishi Chemical Analytech), respectively.

2.2. Materials. To fabricate the electrode, YP-50F activated carbon (Kuraray Co., Ltd.), Ketjenblack (Lion Specialty Chemicals Co., Ltd.), and polyvinylidene fluoride (PVDF) (Sigma-Aldrich, Japan) were used as the active material, the conductive assistant, and the binder, respectively. Tetraethylammonium tetrafluoroborate ($TEABF_4$, >98%, Tokyo Chemical) and propylene carbonate (PC, >99.0%, Kanto Chemical) were used as the supporting electrolyte and solvent for electrochemical measurements, respectively.

2.3. Preparation of Capacitor Electrodes. PVDF (0.0360 g) was added to *N*-methylpyrrolidone (1.80 g) and dissolved by stirring for 24 h. The activated carbon (0.289 g) and the conductive assistant (0.0182 g) were then added in such a way that the weight ratio of activated carbon:conductive assistant:PVDF was 80:5:10. The mixture was stirred for another 3 h to obtain a paste, which was applied to both sides of the SUS fiber sheet (10 mm × 20 mm × 0.1 mmt) or SUS plate (10 mm × 20 mm × 0.8 mmt, SUS316L, Engineering Test Service Co.) using a spatula coated with polytetrafluoroethylene. The area of one coated side was 1 cm^2. The wet coatings were dried using a warm air dryer at 200 °C for 3 h to obtain the capacitor electrodes. The SUS plate was used as a comparison for the SUS fiber sheet. Hereafter, the capacitor electrodes of the SUS fiber sheet and the SUS plate loaded with activated carbon are denoted as capacitor electrodes F and P, respectively. The amount of loaded activated carbon on the capacitor electrode (m) was measured gravimetrically and recorded as the total weight coated on both sides of the 1 cm × 1 cm-sized electrode.

2.4. Electrochemical Measurements. Electrochemical measurements were carried out under a nitrogen atmosphere in a PC solution containing 0.1, 0.5, and 1.0 M $TEABF_4$ using a three-electrode one-compartment type cell (Figure S1 in the Supporting Information). The freshly prepared capacitor electrode and a Pt plate were used as the working and counter electrodes, respectively. All potentials were referenced to an Ag/Ag^+ electrode (RE-7, BAS Inc.).

Cyclic voltammetry was conducted using an electrochemical analyzer (ALS 750A, BAS Inc.) at a sweep rate of 20 mV s^{-1} and a potential range of −0.3 to 1.0 V versus the Ag/Ag^+ reference electrode. The charge−discharge tests employed a charge/discharge unit (HJ1010mSM8A, Hokuto Denko Co.) to galvanostatically charge the capacitor electrodes to 1.0 V and then galvanostatically discharge them to −0.3 V at a current density of 2.0 or 5.0 mA/cm^2.

Electrochemical impedance spectra of the capacitor electrodes were measured with an impedance spectrum analyzer (SP-150, BioLogic) at the discharged state (0 V vs Ag/Ag^+) in a frequency range from 10 mHz to 10 kHz with a potential perturbation of 5 mV.

https://doi.org/10.1021/acsomega.2c00435
ACS Omega 2022, 7, 19216−19224

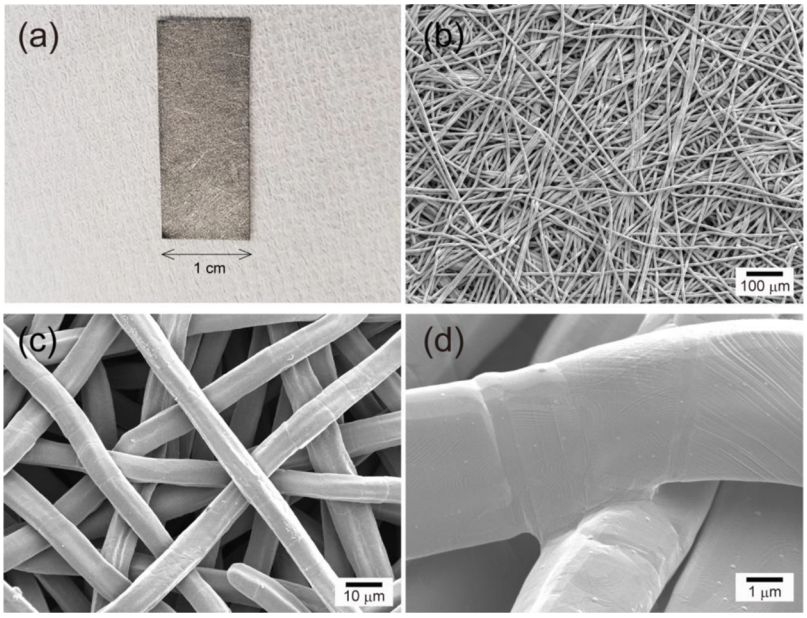

Figure 1. (a) Photograph, (b) low-magnification SEM image, and (c) high-magnification SEM image of the SUS fiber sheet. (d) Enlarged view of a fiber junction.

3. RESULTS AND DISCUSSION

3.1. Morphology of the SUS Fiber Sheet. Figure 1 shows the photograph and SEM images of the as-fabricated SUS fiber sheet. The SEM images reveal a 3D structure formed by entangled fibers. Using the average diameter (8.0 μm), average length (3.0 mm), density (7.98 g cm^{-3}),[37] and basis weight (3.0×10^{-2} g cm^{-2}) of SUS fibers, the actual surface area of an SUS fiber sheet with a geometric area of 1 cm^2 was calculated to be 19 cm^2. A low sheet resistance of 1.5×10^{-1} Ω sq^{-1} was obtained for the fiber sheets because the fibers were bonded to each other by sintering, as shown in Figure 1d.

3.2. Cyclic Voltammetry. Figure 2a shows repeated cyclic voltammograms of the capacitor electrode F and the SUS fiber sheet (solid red and green curves, respectively). The concentration of the supporting electrolyte was 0.1 M, and the amount of loaded carbon was $m = 1.3 \times 10^{-3}$ g/cm^2 geometric area. The SUS fiber sheet showed very little current flow within the measured potential range, indicating its suitability as a current collector. In contrast, the capacitor electrode F showed a large current flow based on the double-layer capacitance. However, the waveform did not have an ideal rectangular shape possibly because the ions cannot easily access the electrode for charging and discharging due to the rate-limiting ion diffusion rate under the given supporting electrolyte concentration and the sweep rate conditions. Figure 2b shows repeated cyclic voltammograms of capacitor electrodes P (solid red and black curves) and the SUS plate (solid green curve), which were also measured in a 0.1 M supporting electrolyte. For the capacitor electrode P, electrodes P1 ($m = 1.3 \times 10^{-3}$ g) and P2 ($m = 7.4 \times 10^{-4}$ g) with different amounts of loaded activated carbon were fabricated. The voltammogram of the capacitor electrode P1 has a smaller response current and a slanted spindle shape compared to that of the capacitor electrode F, which has the same loading of activated carbon. This indicates that ion diffusion has significant effects on the charge/discharge current. In addition, the current gradually decreased with each successive sweep, albeit slightly, suggesting dropouts and exfoliation caused by

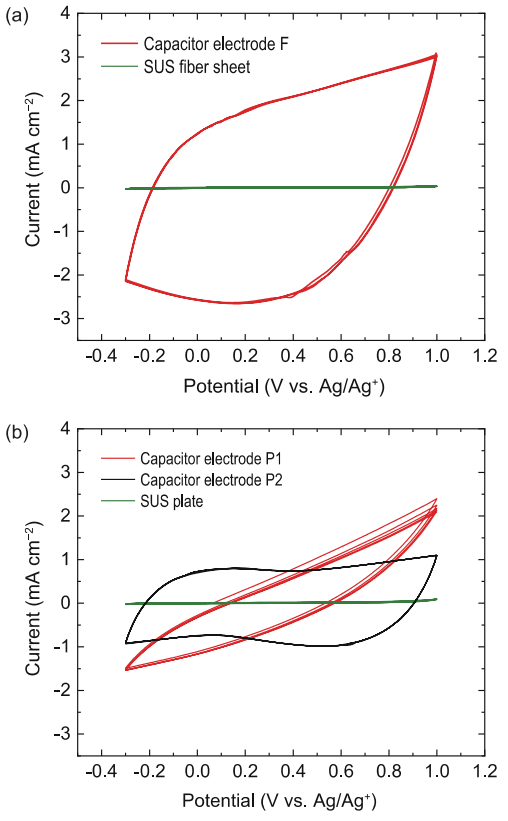

Figure 2. Repeated cyclic voltammograms of (a) capacitor electrode F and the SUS fiber sheet and (b) capacitor electrodes P1 and P2 and the SUS plate. Electrolyte: 0.1 M $TEABF_4$ in PC, sweep rate: 20 mV s^{-1}, and number of potential sweeps: 5.

volume changes in the activated carbon layer during charging and discharging. Information from the voltammograms indicates that it is difficult to form a tight contact between the current collector and the activated carbon layer and that a good conduction path (including ion diffusion pathways) is

https://doi.org/10.1021/acsomega.2c00435
ACS Omega 2022, 7, 19216−19224

not formed when applying a relatively thick activated carbon layer to the SUS plate. On the other hand, the activated carbon mixture was held tightly in the 3D fiber sheet current collector by filling into the pores, leading to a higher amount of activated carbon mixture per unit area. This 3D structure also provides a good conduction path.[31] These factors mentioned above may be responsible for the good current response of the SUS fiber sheet current collector shown in Figure 2a. In support of this interpretation, the voltammogram of the capacitor electrode P2 is closer to a square waveform and displays a slightly higher response current (solid black curve in Figure 2b) compared to the capacitor electrode P1 (solid red curve in Figure 2b). Thus, a reduced amount of activated carbon actually improves the properties of the capacitor electrode P because the activated carbon layer is more firmly retained on the current collector and the ion diffusion is facilitated at a lower active material loading. However, the low loading of activated carbon also led to inferior capacitor properties compared to those of the capacitor electrode F.

The single-electrode specific capacitance (C_m) of the capacitor electrode was estimated using eq 1:[38]

$$C_m = \frac{1}{mv(E_a - E_c)} \int_{E_c}^{E_a} I(E)\mathrm{d}E \quad (1)$$

where $I(E)$ is the cathodic current as a function of the potential E, E_a is the anodic potential limit, E_c is the cathodic potential limit, v is the sweep rate, and m is the mass of activated carbon. Assuming $E_c = -0.3$ V and $E_a = 1.0$ V, the C_m values estimated for the voltammograms in Figure 2 were 74, 22, and 50 F g^{-1} for capacitor electrodes F, P1, and P2, respectively.

Figure 3 shows the repeated cyclic voltammograms of the capacitor electrode F at different supporting electrolyte concentrations (0.1, 0.5, and 1.0 M; the data at 0.1 M were reproduced from Figure 2). These voltammograms develop a more rectangular shape at higher electrolyte concentrations, indicating easier access of ions to the electrode. In addition to the waveform change, the voltammogram profiles develop a butterfly shape: the current increases in both the negative and positive sides from a potential of ~0.3 V versus Ag/Ag$^+$ (where the current is at local minimum). Two models could explain the butterfly-shaped EDLC voltammograms.[14,39,40] One explanation is that the potential corresponding to the minimum current is the point of zero charge (pzc), and charging and discharging proceed by adsorption of anions and cations at potentials more positive and negative than pzc, respectively. When different ion species are involved in charging and discharging, the structure of the Helmholtz layer changes, which affects the capacitance. Thus, the voltammogram changes shape at potentials above and below the pzc. Another explanation is that the space charge layer on the electrode side changes depending on the potential. However, such a semiconducting behavior does not apply to this study because the density of charge carriers in activated carbon is sufficiently high compared to the density of ion carriers on the electrolyte side. Therefore, we believe that the butterfly-shaped voltammograms in Figure 3 are better explained by the former model. This also indicates that the pore structure in the material is capable of transporting both anions and cations.[41]

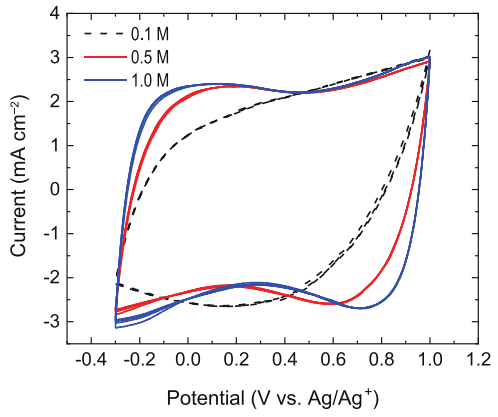

Figure 3. Repeated cyclic voltammograms of the capacitor electrode F measured in 0.1, 0.5, and 1.0 M $TEABF_4$ in PC. Sweep rate: 20 mV s^{-1} and number of potential sweeps: 5.

The same approach was used to estimate C_m for the capacitor electrode F at the supporting electrolyte concentrations of 0.5 and 1.0 M. The obtained C_m values (83 and 90 F g^{-1}, respectively) suggest that ion diffusion is improved when using a more concentrated supporting electrolyte.

3.3. Constant Current Density Charge/Discharge Tests and Cycle-Life Performance. To highlight the capacitance characteristics of the different capacitor electrodes, constant current density charge/discharge tests were carried out. Figure 4a,b show the charge and discharge curves (i.e., potential(E)−time(t) response) for capacitor electrodes F and P2, respectively, using a 0.1 M supporting electrolyte and a current density of 2.0 mA cm^{-2}. The number of charge/discharge cycles was set to 1000. For the reasons discussed in Section 3.2, the capacitor electrode P2 was employed here as a comparison instead of the capacitor electrode P1 that carries the same amount of activated carbon as the capacitor electrode F. Both E−t responses showed the typical capacitance behavior with a triangular wave shape, indicating that reversible charging−discharging took place. When switching from charging to discharging, an IR drop was observed in both capacitor electrodes, especially in capacitor electrode P2. As will be described in detail later in Section 3.4, the charging of the electric double layer in the capacitor electrode P2 is not dominated by the capacitive component but rather limited by ion diffusion, which leads to a larger IR drop. The value of C_m was calculated according to eq 2 from the E−t responses in Figure 4a,b.[42−44]

$$C_m = \frac{I \times \Delta t}{\Delta V \times m} \quad (2)$$

where I is the discharge current, Δt is the discharge time, and ΔV is the potential drop during the discharge process. In particular, C_m was calculated from the slope of the discharge lines excluding the IR drop. The initial C_m values for capacitor electrodes F and P2 were 95 and 51 F g^{-1}, respectively. For the capacitor electrode F, its cyclic voltammogram did not have an ideal rectangle shape (as shown in Figure 2a). Accordingly, the capacitance value calculated from Figure 4 was slightly different from that calculated from Figure 2a. Figure 4c,d show the E−t responses recorded in 0.5 and 1.0 M $TEABF_4$ supporting electrolyte, respectively. As the supporting electrolyte concentration was increased, the IR drop decreased, indicating that one of the causes is a lower bulk resistance in the electrolyte. The initial C_m values of the capacitor electrode F in 0.5 and 1.0 M $TEABF_4$ were 97 and 99 F g^{-1}, respectively.

https://doi.org/10.1021/acsomega.2c00435
ACS Omega 2022, 7, 19216−19224

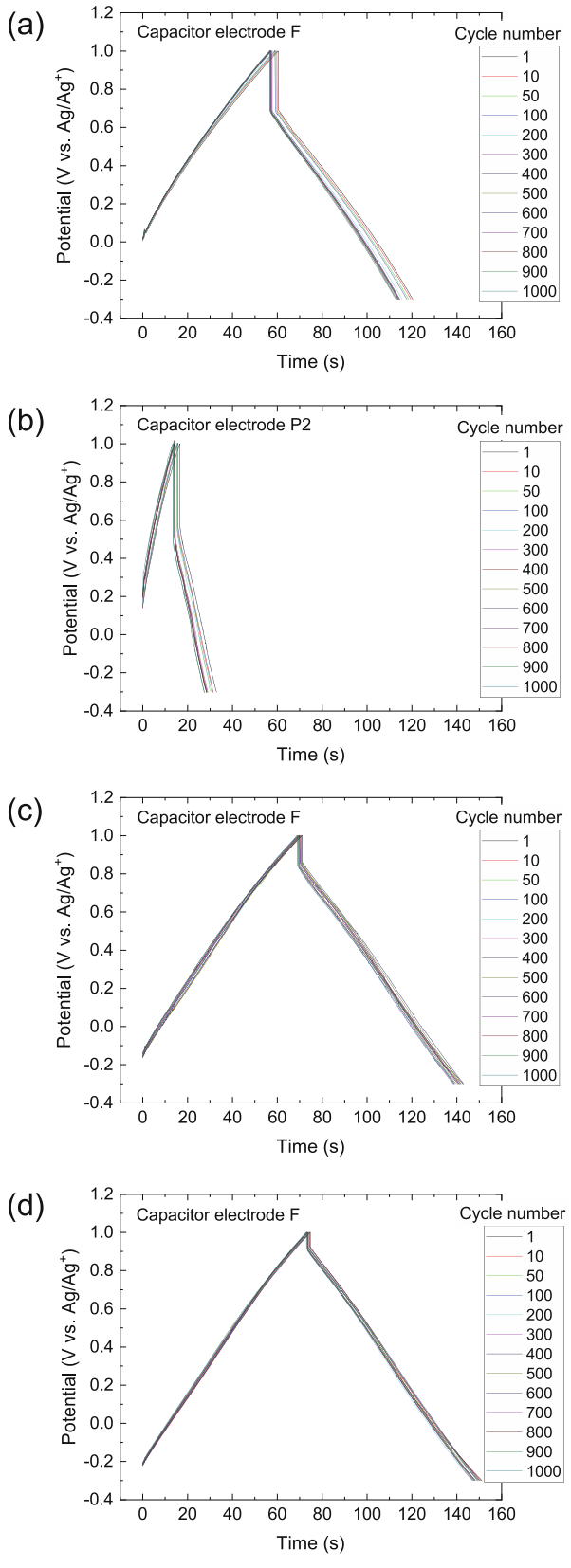

Figure 4. Constant current density charge/discharge test (potential–time (E–t) curves) for the capacitor electrode F measured in PC containing (a) 0.1, (c) 0.5, and (d) 1.0 M $TEABF_4$. For comparison, panel (b) shows the E–t curves of the capacitor electrode P2 measured in PC containing 0.1 M $TEABF_4$. Charge and discharge current density: 2.0 mA cm^{-2}.

Figure 5a shows the results of the cycle-life test for the capacitor electrodes. All electrodes displayed good capacity

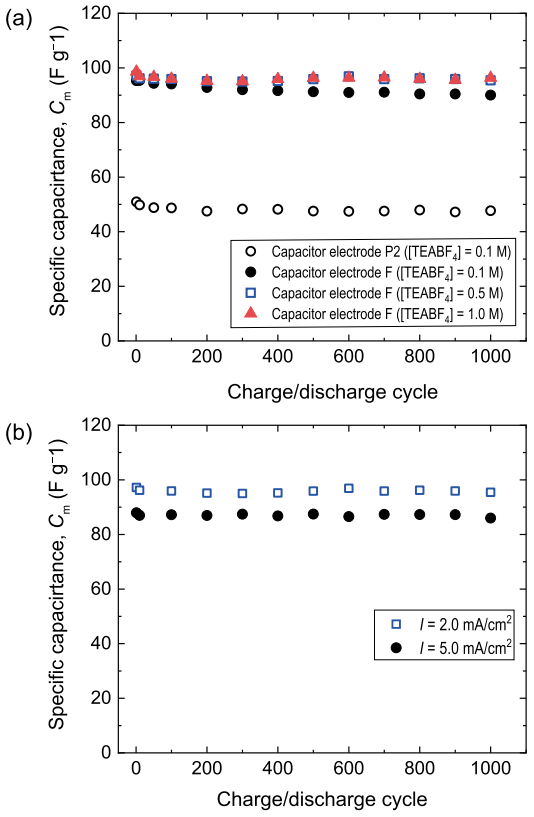

Figure 5. (a) Dependence of C_m on the charge/discharge cycle number for the capacitor electrode F measured in PC containing 0.1, 0.5, and 1.0 M $TEABF_4$. The current density was 2.0 mA cm^{-2}. For comparison, the C_m values of the capacitor electrode P2 measured in PC containing 0.1 M $TEABF_4$ is also shown. (b) Dependence of C_m on the cycle number for the capacitor electrode F measured in PC containing 0.5 M $TEABF_4$. The current densities were 2.0 and 5.0 mA cm^{-2}.

retention characteristics. After 1000 cycles, the capacitance decay ratio for the capacitor electrode P2 was 6.4%, while those for the capacitor electrode F in 0.1, 0.5, and 1.0 M $TEABF_4$ were 5.5, 1.8, and 2.3%, respectively, indicating that the fiber sheet-type current collector has extremely high durability. Figure 5b shows the dependence of C_m on the discharge current rate for the capacitor electrode F in 0.5 M $TEABF_4$. At a current density of 5.0 mA cm^{-2}, the electrode retained 90% of its capacity at 2.0 mA cm^{-2}. In addition, the capacitance decay ratio was only 2.2% after 1000 cycles at 5.0 mA cm^{-2}. These results demonstrate the superior ability of the fiber sheet substrate for collecting current.

3.4. Electrochemical Impedance Measurement. To investigate the performance of the capacitor electrodes in detail, electrochemical impedance measurements were performed to distinguish the resistance and capacitance of each electrode. Figure 6 shows the Nyquist plot for capacitor electrodes F and P2, namely, the imaginary part of the complex impedance ($-Z_{im}$) versus the real part (Z_{re}). The plot for the capacitor electrode F consists of a semicircle at high frequencies between points A and B, a nonvertical line at intermediate frequencies between points B and C, and a nearly vertical line at low frequencies beyond point C. In contrast, the

https://doi.org/10.1021/acsomega.2c00435
ACS Omega 2022, 7, 19216–19224

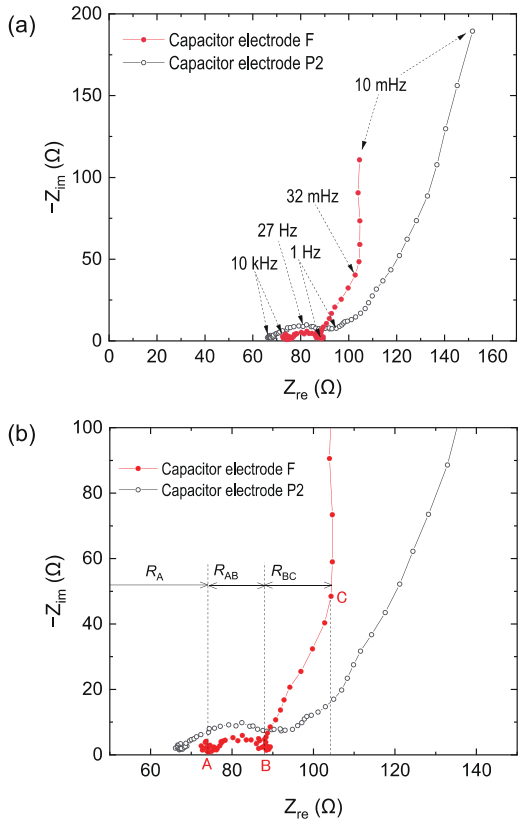

Figure 6. (a) Nyquist plots of capacitor electrodes F and P2. (b) A magnified view of panel (a). The measurements were performed in PC containing 0.1 M $TEABF_4$.

capacitor electrode P2 did not display the vertical line at low frequencies. The vertical line indicates that the capacitive component dominates the charging process of the electric double layer at the electrode/electrolyte interface. Therefore, its absence (due to the extension of the region between points B and C) means that the charging process is limited by ion diffusion.[45] According to Mei et al., the resistance R_{BC} in this region corresponds to the diffuse layer resistance.[45]

Several models have been proposed to assign the semicircle diameter (resistance R_{AB} in Figure 6b). Some studies attributed it to the resistance of the electrolyte in the porous electrode structure.[46−48] The capacitor electrode F has a smaller R_{AB} than the capacitor electrode P2 due to the following possible reasons. The capacitor electrode F contains finely branched spaces created by the metal fibers and the active material inside the electrode. Therefore, it is expected to provide fast ion transport channels with short diffusion pathways, which would lower the diffusion resistance of ions in that space. To confirm this, the cross section of the capacitor electrode F was observed by SEM. In the image shown in Figure 7, the white structures are the SUS fibers, and the nearby particulate structures in a slightly darker shade are the electrode active materials. There are also cone-shaped pointy structures extending downward from the periphery of the SUS fibers, which were regarded as uneven artifacts created during sample processing. After the sample was embedded in resin, the surface was etched by argon gas prior to observation. The different etching rates of SUS and resin probably caused the uneven shapes to form during this step. The SEM image confirmed that the electrode active materials penetrated the fiber sheet and clung to the fibers.

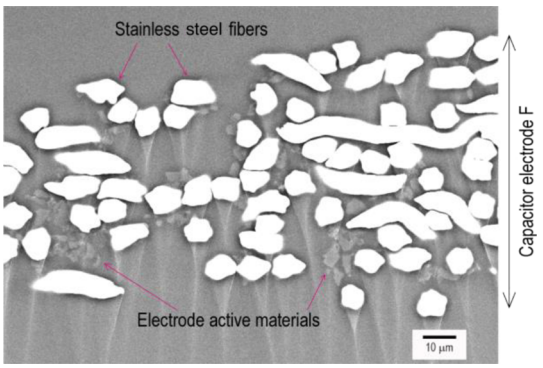

Figure 7. Cross-sectional SEM image of the capacitor electrode F.

Therefore, many contact points were formed between the metal fibers and the active material particles, and finely branched spaces near these contact points could enable fast ion transport. Figure 8a shows the Nyquist plots of the capacitor electrode F at different supporting electrolyte concentrations. Upon increasing the supporting electrolyte concentration, the effect of fast ion transport described above probably became more pronounced, resulting in a significant decrease in the ion diffusion resistance (R_{AB}) and a markedly smaller diameter of the semicircle.

In Figure 6b, the resistance R_A of the capacitor electrode F (indicated by the distance from the origin to point A) is slightly larger than that of the capacitor electrode P2. According to Figure 8a, R_A should include the bulk electrolyte resistance because it decreased significantly in a more concentrated supporting electrolyte. However, the fact that R_A is larger for the capacitor electrode F than for P2 at the same bulk electrolyte resistance indicates that factors other than the bulk electrolyte resistance also contribute to R_A. Most likely, R_A is the sum of the bulk electrolyte resistance, the resistance of the electrode active materials, and the contact resistance between the active materials and the current collector.[47−51] As shown in Figure 7, the electrode active materials in the capacitor electrode F contact the current collector at many points, while there are fewer contacts in the capacitor electrode P2 employing a flat plate as the current collector. Therefore, the contact resistance would be lower in the former case. On the other hand, because the capacitor electrode F has a higher loading of electrode active materials than the capacitor electrode P2, the corresponding resistance component should be larger. Considering the factors mentioned above, we conclude that the R_A value of the capacitor electrode F is somewhat larger than that of the capacitor electrode P2 because the higher active material loading in the former more than canceled the reduction in contact resistance.

To examine the diffusion process of ions in the electrolyte, we replotted the data in Figure 8a as $-Z_{im}$ versus $Z_{re} - R_A$ in Figure 8b. It has been mentioned that increasing the supporting electrolyte concentration decreased the values of R_A and R_{AB}. In addition, when the supporting electrolyte concentration was 0.5 and 1.0 M, points B and C overlapped and there was almost no region showing the diffusion resistance R_{BC}. The reason is that a highly concentrated electrolyte reduces the thickness of the diffusion layer.[45] Figure 8c shows the enlarged semicircle region of Figure 8b. As the concentration of the supporting electrolyte was increased, the diameter of the semicircle (or R_{AB}) decreased. This implies

https://doi.org/10.1021/acsomega.2c00435
ACS Omega 2022, 7, 19216−19224

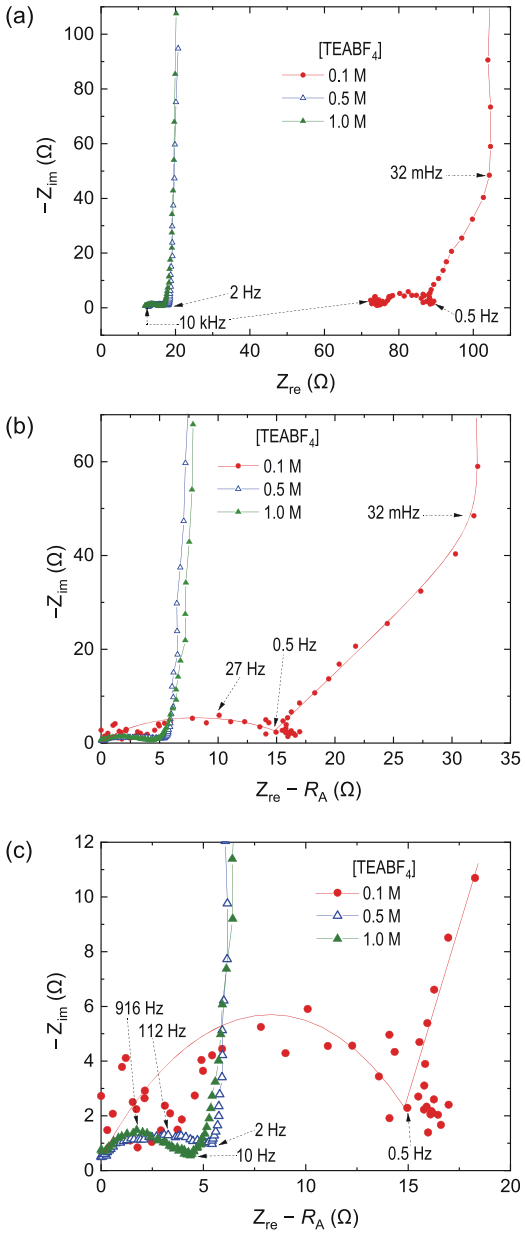

Figure 8. (a) Nyquist plot for the capacitor electrode F at $TEABF_4$ concentrations of 0.1, 0.5, and 1.0 M. (b) Modified Nyquist plot ($-Z_{im}$ versus $Z_{re} - R_A$) for the three electrolyte concentrations. (c) A magnified view of panel (b).

that the ion diffusion path became shorter in the finely branched space formed inside the electrode upon increasing the supporting electrolyte concentration.

Table 1 summarizes the values of R_A, R_{AB}, and R_{BC} calculated from the AC impedance responses (Figures 6 and 8) of capacitor electrodes F and P2. The internal resistance R and the specific capacitance C_m calculated from Figure 4 are also listed in the table. The capacitor electrode F displayed significantly smaller R_A, R_{AB}, R_{BC}, and R and relatively larger C_m values at $[TEABF_4]$ = 0.5 and 1.0 M due to the reasons mentioned above. Note that $R \neq R_A + R_{AB} + R_{BC}$. According to previous studies,[22,52,53] this difference is due to the diffusion resistance of ions in the micropores of activated carbon, and it makes a larger contribution to the *IR* drop than R_A, R_{AB}, and R_{BC}.

Table 1. Capacitor Performances of Capacitor Electrodes F and P2

electrode	$[TEABF_4]$ (M)	R_A (Ω)	R_{AB} (Ω)	R_{BC} (Ω)	R (Ω)	C_m (F g^{-1})
capacitor electrode F	0.1	73.6	15.2	14.4	156	95
capacitor electrode F	0.5	12.6	5.3	~0	70	97
capacitor electrode F	1.0	11.8	4.3	~0	38	99
capacitor electrode P2	0.1	66.7	26.4	>150	215	51

These results suggest that the superior performance of the capacitor electrode F over the capacitor electrode P2 is due to two reasons: (1) the shorter ion diffusion length caused by the finely branched space formed by the fibrous current collector and the electrode active material and (2) the lower contact resistance due to more contact points formed between the current collector and the active material.

4. CONCLUSIONS

SUS fiber sheets with a 3D porous structure were fabricated using a relatively facile method for use as a current collector in an EDLC. The EDLC electrode using this current collector was found to hold a larger amount of active material than the electrode using a flat SUS plat as the current collector and has a larger capacitance value. Furthermore, the EDLC electrode showed excellent charge−discharge characteristics, including cycle performance and rate capability. Based on the results of electrochemical impedance measurements, these advantages of the EDLC electrode using the SUS fiber sheet current collector can be attributed to a larger number of contact points formed between the fibers and the active material as well as the shorter diffusion length of ions in the finely branched space created by the fibers and the active material. Compared to the previously reported current collectors with 3D structures, our SUS fiber sheet was fabricated with less effort and at a lower cost. In the future, we plan to extend this structure to other metals. We are also applying the SUS fiber sheet current collector to redox capacitors in which the active material itself exhibits redox responses.

■ ASSOCIATED CONTENT

Supporting Information

The Supporting Information is available free of charge at https://pubs.acs.org/doi/10.1021/acsomega.2c00435.

Electrochemical cell used for measurements (Figure S1) (PDF)

■ AUTHOR INFORMATION

Corresponding Author

Katsuyoshi Hoshino − *Department of Materials Sciences, Graduate School of Engineering, Chiba University, Chiba 263-8522, Japan;* orcid.org/0000-0002-4740-3486; Email: k_hoshino@faculty.chiba-u.jp

Authors

Daisuke Muramatsu − *Department of Materials Sciences, Graduate School of Engineering, Chiba University, Chiba 263-8522, Japan; iCas Company Research & Development Div., Tomoegawa Co.,Ltd., Shizuoka 421-0192, Japan*

https://doi.org/10.1021/acsomega.2c00435
ACS Omega 2022, 7, 19216−19224

Keisuke Masunaga − *Department of Materials Sciences, Graduate School of Engineering, Chiba University, Chiba 263-8522, Japan*
Aoi Magori − *Department of Materials Sciences, Graduate School of Engineering, Chiba University, Chiba 263-8522, Japan*
Satoru Tsukada − *Department of Materials Sciences, Graduate School of Engineering, Chiba University, Chiba 263-8522, Japan;* orcid.org/0000-0003-0175-6152

Complete contact information is available at: https://pubs.acs.org/10.1021/acsomega.2c00435

Notes

The authors declare no competing financial interest.

■ ACKNOWLEDGMENTS

We would like to thank the iCas company of Tomoegawa Paper Co., Ltd. and their analysis center for their help in preparing the fiber sheets and the SEM measurements, respectively.

■ REFERENCES

(1) Inagaki, M.; Konno, H.; Tanaike, O. Carbon Materials for Electrochemical Capacitors. *J. Power Sources* **2010**, *195*, 7880−7903.
(2) Muzaffar, A.; Ahamed, M. B.; Deshmukh, K.; Thirumalai, J. A Review on Recent Advances in Hybrid Supercapacitors: Design, Fabrication and Applications. *Renew. Sustain. Energy Rev.* **2019**, *101*, 123−145.
(3) Nishino, A. Capacitors: Operating Principles, Current Market and Technical Trends. *J. Power Sources* **1996**, *60*, 137−147.
(4) Zhao, J.; Burke, A. F. Review on Supercapacitors: Technologies and Performance Evaluation. *J. Energy Chem.* **2021**, *59*, 276−291.
(5) Endo, M.; Takeda, T.; Kim, Y. J.; Koshiba, K.; Ishii, K. High Power Electric Layer Capacitor (EDLC's); from Operating Principle to Pore Size Control in Advanced Activated Carbons. *Carbon Lett.* **2001**, *1*, 117−128.
(6) Pognon, G.; Brousse, T.; Bélanger, D. Effect of Molecular Grafting on the Pore Size Distribution and the Double Layer Capacitance of Activated Carbon for Electrochemical Double Layer Capacitors. *Carbon* **2011**, *49*, 1340−1348.
(7) Miller, J. R.; Outlaw, R. A.; Holloway, B. C. Graphene Electric Double Layer Capacitor with Ultra-High-Power Performance. *Electrochim. Acta* **2011**, *56*, 10443−10449.
(8) du, X.; Guo, P.; Song, H.-H.; Chen, X. Graphen Nanosheets as Electrode Material for Electric Double-Layer Capacitors. *Electrochim. Acta* **2010**, *55*, 4812−4819.
(9) Huang, Y.-F.; Wu, P.-F.; Zhang, M.-Q.; Ruan, W.-H.; Giannelis, E. P. Boron Cross-Linked Graphene Oxide/Polyvinyl Alcohol Nanocomposite Gel Electrolyte for Flexible Solid-State Electric Double Layer Capacitor with High Performance. *Electrochim. Acta* **2014**, *132*, 103−111.
(10) Jung, M.-J.; Jeong, E.; Lee, Y.-S. The Surface Chemical Properties of Multi-Walled Carbon Nanotubes Modified by Thermal Fluorination for Electric Double-Layer Capacitor. *Appl. Surf. Sci.* **2015**, *347*, 250−257.
(11) Shiraishi, S.; Kurihara, H.; Okabe, K.; Hulicova, D.; Oya, A. Electric Double Layer Capacitance of Highly Pure Single-Walled Carbon Nanotubes (HiPco^{TM} Buckytubes^{TM}) in Propylene Carbonate Electrolytes. *Electrochem. Commun.* **2002**, *4*, 593−598.
(12) Li, C.; Wang, D.; Liang, T.; Wang, X.; Ji, L. A Study of Activated Carbon Nanotubes as Double-Layer Capacitors Electrode Materials. *Mater. Lett.* **2004**, *58*, 3774−3777.
(13) Huang, C.-W.; Hsieh, C.-T.; Kuo, P.-L.; Teng, H. Electric Double Layer Capacitors Based on a Composite Electrode of Activated Mesophase Pitch and Carbon Nanotubes. *J. Mater. Chem.* **2012**, *22*, 7314−7322.
(14) Kimizuka, O.; Tanaike, O.; Yamashita, J.; Hiraoka, T.; Futaba, D. N.; Hata, K.; Machida, K.; Suematsu, S.; Tamamitsu, K.; Saeki, S.; Yamada, Y.; Hatori, H. Electrochemical Doping of Pure Single-Walled Carbon Nanotubes Used as Supercapacitor Electrodes. *Carbon* **2008**, *46*, 1999−2001.
(15) Izadi-Najafabadi, A.; Yamada, T.; Futaba, D. N.; Yudasaka, M.; Takagi, H.; Hatori, H.; Iijima, S.; Hata, K. High-Power Supercapacitor Electrodes from Single-Walled Carbon Nanohorn/Nanotube Composite. *ACS Nano* **2011**, *5*, 811−819.
(16) Li, Y.; Chen, C. Polyaniline/Carbon Nanotubes-Decorated Activated Carbon Fiber Felt as High-Performance, Free-Standing and Flexible Supercapacitor Electrodes. *J. Mater. Sci.* **2017**, *52*, 12348−12357.
(17) Morimoto, T.; Hiratsuka, K.; Sanada, Y.; Kurihara, K. Electric Double-Layer Capacitor Using Organic Electrolyte. *J. Power Sources* **1996**, *60*, 239−247.
(18) Ishikawa, M.; Morita, M.; Ihara, M.; Matsuda, Y. Electric Double-Layer Capacitor Composed of Activated Carbon Fiber Cloth Electrodes and Solid Polymer Electrolytes Containing Alkylammonium Salts. *J. Electrochem. Soc.* **1994**, *141*, 1730−1734.
(19) Wada, H.; Yoshikawa, K.; Nohara, S.; Furukawa, N.; Inoue, H.; Sugoh, N.; Iwasaki, H.; Iwakura, C. Electrochemical Characteristics of New Electric Double Layer Capacitor with Acidic Polymer Hydrogel Electrolyte. *J. Power Sources* **2006**, *159*, 1464−1467.
(20) Yamazaki, S.; Takegawa, A.; Kaneko, Y.; Kadokawa, J.; Yamagata, M.; Ishikawa, M. An Acidic Cellulose-Chitin Hybrid Gel as Novel Electrolyte for an Electric Double Layer Capacitor. *Electrochem. Commun.* **2009**, *11*, 68−70.
(21) Senthilkumar, S. T.; Selvan, R. K.; Melo, J. S.; Sanjeeviraja, C. High Performance Solid-State Electric Double Layer Capacitor From Redox Mediated Gel Polymer Electrolyte and Renewable Tamarind Fruit Shell Derived Porous Carbon. *ACS Appl. Mater. Interfaces* **2013**, *5*, 10541−10550.
(22) Liu, X.; Osaka, T. Properties of Electric Double Layer Capacitors with Various Polymer Gel Electrolytes. *J. Electrochem. Soc.* **1997**, *144*, 3066−3071.
(23) Fan, L.-Q.; Zhong, J.; Wu, J.-H.; Lin, J.-M.; Huang, Y.-F. Improving the Energy Density Of Quasi-Solid-State Electric Double-Layer Capacitors by Introducing Redox Additives into Gel Polymer Electrolytes. *J. Mater. Chem. A* **2014**, *2*, 9011−9014.
(24) Josef, E.; Yan, R.; Guterman, R.; Oschatz, M. Electrospun Carbon Fibers Replace Metals as a Current Collector in Supercapacitors. *ACS Appl. Energy Mater.* **2019**, *2*, 5724−5733.
(25) Nian, J.-N.; Teng, H. Influence of the Semiconducting Properties of Current Collector on the Electric Double Layer Formation on Porous Carbon. *J. Phys. Chem. B* **2005**, *109*, 10279−10284.
(26) Matsumoto, I.; Ikeyama, M.; Iwaki, T.; Ogawa, H. Studies on the Utilization of Formed Nickel Positive Plate. *Denki Kagaku* **1986**, *54*, 159−163.
(27) Obodo, R. M.; Shinde, N. M.; Chime, U. K.; Ezugwu, S.; Nwanya, A. C.; Ahmad, I.; Maaza, M.; Ejikeme, P. M.; Ezema, F. I. Recent Advances in Metal Oxide/Hydroxide on Three-Dimensional Nickel Foam Substrate for High Performance Pseudocapacitive Electrodes. *Curr. Opin. Electrochem.* **2020**, *21*, 242−249.
(28) García-Moreno, F. Commercial Applications of Metal Foams: Their Properties and Production. *Materials* **2016**, *9*, 85.
(29) Lu, X.; Lin, W.-L.; Huang, Y.-E.; Zhang, J.-X.; Guan, L.-H.; Huang, X.-Y.; Du, K.-Z.; Wu, X.-H. Boosting Potassium Storage Performance of Red Phosphorous via Modifying the Nickel Foam Substrate. *ACS Appl. Energy Mater.* **2021**, *4*, 9682−9691.
(30) Yao, M.; Okuno, K.; Iwaki, T.; Kato, M.; Tanase, S.; Emura, K.; Sakai, T. High-Capacity Electric Double Layer Capacitor Using Three-Dimensional Porous Current Collector. *Electrochem. Solid State Lett.* **2007**, *10*, A245−A249.
(31) Abe, H.; Kubota, M.; Nemoto, M.; Masuda, Y.; Tanaka, Y.; Munakata, H.; Kanamura, K. High-Capacity Thick Cathode with a Porous Aluminum Current Collector for Lithium Secondary Batteries. *J. Power Sources* **2016**, *334*, 78−85.

(32) Hirota, N.; Okuno, K.; Majima, M.; Hosoe, A.; Uchida, S.; Ishikawa, M. High-Performance Lithium-Ion Capacitor Composed of Electrodes with Porous Three-Dimensional Current Collector and Bis(fluorosulfonyl)Imide-Based Ionic Liquid Electrolyte. *Electrochim. Acta* **2018**, *276*, 125−133.
(33) Sakaida, H.; Goto, K.; Kimura, K.; Okuno, K.; Nishimura, J.; Hosoe, A. Aluminum-Celmet−Aluminum Porous Metal with Three-Dimensional Consecutive Pores. *SEI Tech. Rev.* **2017**, *84*, 87−92.
(34) Huang, Y.; Li, Y.; Gong, Q.; Zhao, G.; Zheng, P.; Bai, J.; Gan, J.; Zhao, M.; Shao, Y.; Wang, D.; Liu, L.; Zou, G.; Zhuang, D.; Liang, J.; Zhu, H.; Nan, C. Hierarchically Mesostructured Aluminum Current Collector for Enhancing the Performance of Supercapacitors. *ACS Appl. Mater. Interfaces* **2018**, *10*, 16572−16580.
(35) Fibribond. http://sansho.co.jp/en/find/chemicalfiber/fibribond/ (accessed 2022-01-12).
(36) Lee, L.H. Microstructures and Physical Properties of Synthetic and Modified Papers. In *Scanning Electron Microscopy of Polymers and Coatings II*; Princen, L. H., Ed.; John Willey & Sons, 1974; 166−179.
(37) Park, K.; Park, J.; Kwon, H. Fabrication and Characterization of Al-SUS316L Composite Materials Manufactured by the Spark Plasma Sintering Process. *Mater. Sci. Eng. A* **2017**, *691*, 8−15.
(38) Srinivasan, V.; Weidner, J. W. Capacitance Studies of Cobalt Oxide Films Formed via Electrochemical Precipitation. *J. Power Sources* **2002**, *108*, 15−20.
(39) Ruch, P. W.; Kötz, R.; Wokaun, A. Electrochemical Characterization of Single-Walled Carbon Nanotubes for Electrochemical Double Layer Capacitors Using Non-Aqueous Electrolyte. *Electrochim. Acta* **2009**, *54*, 4451−4458.
(40) Tanaike, O.; Futaba, D. N.; Hata, K.; Hatori, H. Supercapacitors Using Pure Single-Walled Carbon Nanotubes. *Carbon Lett.* **2009**, *10*, 90−93.
(41) Kötz, R.; Hahn, M.; Barbieri, O.; Sauter, J.-C.; Gallay, R. The Electronic Side of The Double-Layer: Impact on Diagnostics and Improvement of Carbon Double Layer Electrodes. In *Proceedings of the 13th International Seminar on Double Layer Capacitors and Similar Energy Storage Devices*, Deerfield Beach, USA, December 8−10, 2003.
(42) Yuan, C.; Zhang, X.; Gao, B.; Li, J. Synthesis and Electrochemical Capacitance of Mesoporous $Co(OH)_2$. *Mater. Chem. Phys.* **2007**, *101*, 148−152.
(43) Zhou, W.-J.; Zhao, D.-D.; Xu, C. L.; Xu, C. L.; Li, H. L. Effects of the Electrodeposition Potential and Temperature on the Electrochemical Capacitance Behavior of Ordered Mesoporous Cobalt Hydroxide Films. *Electrochim. Acta* **2008**, *53*, 7210−7219.
(44) Hu, Z.; Mo, L.; Feng, X.; Shi, J.; Wang, Y.; Xie, Y. Synthesis and Electrochemical Capacitance of Sheet-Like Cobalt Hydroxide. *Mater. Chem. Phys.* **2009**, *114*, 53−57.
(45) Mei, B.-A.; Munteshari, O.; Lau, J.; Dunn, B.; Pilon, L. Physical Interpretations of Nyquist Plots for EDLC Electrodes and Devices. *J. Phys. Chem. C* **2018**, *122*, 194−206.
(46) Fang, B.; Binder, L. A Modified Activated Carbon Aerogel for High-Energy Storage in Electric Double Layers. *J. Power Sources* **2006**, *163*, 616−622.
(47) Liu, C.-L.; Dong, W.-S.; Cao, G.-P.; Song, J.-R.; Liu, L.; Yang, Y.-S. Influence of KOH Followed by Oxidation Pretreatment on the Electrochemical Performance of Phenolic Based Activated Carbon Fibers. *J. Electroanal. Chem.* **2007**, *611*, 225−231.
(48) Gamby, J.; Taberna, P. L.; Simon, P.; Fauvarque, J. F.; Chesneau, M. Studies and Characterisations of Various Activated Carbons Used for Carbon/Carbon Supercapacitors. *J. Power Sources* **2001**, *101*, 109−116.
(49) Kötz, R.; Carlen, M. Principles and Applications of Electrochemical Capacitors. *Electrochim. Acta* **2000**, *45*, 2483−2498.
(50) Portet, C.; Yushin, G.; Gogotsi, Y. Electrochemical Performance of Carbon Onions, Nanodiamonds, Carbon Black and Multiwalled Nanotubes in Electrical Double Layer Capacitors. *Carbon* **2007**, *45*, 2511−2518.
(51) Lufrano, F.; Staiti, P.; Minutoli, M. Evaluation of Nafion Based Double Layer Capacitors by Electrochemical Impedance Spectroscopy. *J. Power Sources* **2003**, *124*, 314−320.
(52) Teng, H.; Chang, Y.-J.; Hsieh, C.-T. Performance of Electric Double-Layer Capacitors Using Carbons Prepared from Phenol−Formaldehyde Resins by KOH Etching. *Carbon* **2001**, *39*, 1981−1987.
(53) Qiao, W.; Yoon, S.-H.; Mochida, I. KOH Activation of Needle Coke to Develop Activated Carbons for High-Performance EDLC. *Energy Fuels* **2006**, *20*, 1680−1684.

https://doi.org/10.1021/acsomega.2c00435
ACS Omega 2022, 7, 19216−19224